

Communication

Revealing the Synergetic Effects between Reactants in Oxidative Coupling of Methane on Stepped MgO(100) Catalyst

Xiaoying Sun ¹, Yue Liu ¹, Xinyu Li ¹, Zhan Yu ¹ , Bo Li ¹ and Zhen Zhao ^{1,2,*}

¹ Institute of Catalysis for Energy and Environment, College of Chemistry and Chemical Engineering, Shenyang Normal University, Shenyang 110034, China

² State Key Laboratory of Heavy Oil Processing, China University of Petroleum, Beijing 102249, China

* Correspondence: zhaozhen1586@163.com or zhenzhao@cup.edu.cn or zhaozhen@synu.edu.cn

Abstract: The oxidative coupling of methane (OCM) on MgO is often computationally explored via Mars-Krevelen (MvK) mechanism. However, the difficult desorption of CH₃ radical at stepped MgO surface shadow the feasibility of mechanism. In this work, density functional theory calculations are performed to unravel the synergetic effects between reactants which lead to a new Langmuir-Hinshelwood (L-H)-like mechanism. It was found that co-adsorption of reactants pave ways for CH₃ radical formation with negligible desorption energy. The role of oxygen molecule is not only to oxidize reduced surface but also decrease the reactivity of Mg-O site which facile CH₃ desorption. Electronic structure analysis indicated the distinct feature along pathway between MvK and L-H. The current work clearly indicated the importance of effective interactions between reactants and provided new insights on the reaction mechanism of OCM.

Keywords: oxidative coupling of methane; mechanism; DFT; doping



Citation: Sun, X.; Liu, Y.; Li, X.; Yu, Z.; Li, B.; Zhao, Z. Revealing the Synergetic Effects between Reactants in Oxidative Coupling of Methane on Stepped MgO(100) Catalyst. *Catalysts* **2022**, *12*, 903. <https://doi.org/10.3390/catal12080903>

Academic Editors: Guangchao Liang and Charles Edwin Webster

Received: 23 July 2022

Accepted: 15 August 2022

Published: 17 August 2022

Publisher's Note: MDPI stays neutral with regard to jurisdictional claims in published maps and institutional affiliations.



Copyright: © 2022 by the authors. Licensee MDPI, Basel, Switzerland. This article is an open access article distributed under the terms and conditions of the Creative Commons Attribution (CC BY) license (<https://creativecommons.org/licenses/by/4.0/>).

1. Introduction

With rising of Shale gas revolution worldwide, the supply of abundant of methane spurred the urgent needs for highly effective conversion of methane to value-added chemical commodities such as ethane, ethylene and methanol etc. which have apparent importance for both academic research and economic applications [1–3]. Due to its high symmetry and strong C-H bond, the conversion of methane is one of most challenging catalytic process. This process has been deemed as “golden grail” in heterogeneous catalysis [4]. In fact, there are many attempts to catalyze methane molecule in various ways including partial oxidation, aromatization, steam/dry reformation, and halogenation etc. which achieved certain success with fine-tuned catalysts [5].

Among them, oxidative coupling of methane (OCM) is one of dream reactions which directly convert methane to C₂ products such as ethane and ethylene which are building blocks of entire chemistry industry [6–8]. OCM can be sketchily described as three steps: (i). Generation of CH₃ radicals on catalyst surface; (ii). The coupling of CH₃ radicals to form ethane; (iii). The conversion between ethane and ethylene [9]. The current major obstacles of OCM are that the yield of C₂ products is rather low and the side reactions are difficult to control. These two aspects are in fact intertwined together. The exploration of novel catalysts is always an important method to circumvent the bottleneck of OCM. Conventionally, the catalysts of OCM included high basic lanthanide oxide such as La₂O₃ [10–12], doped alkaline earth metal oxides such as Li/MgO [13,14]. It is generally suggested that strong basicity is key element to guarantee the catalytic performance [15–17].

Li doped MgO (Li/MgO) is one of most studied OCM catalysts ever. For the first time, Lunsford et al. found that Li/MgO has a good performance in OCM in 1980's [18]. They also proposed that Li doping is essential to create site for oxygen molecule activation which is considered to be key step in OCM. The active center, Li⁺-O⁻ was identified from ESR measurement [19]. Moreover, methane underwent a homolytic dissociation to produce

CH₃ radical. On the other hand, it was proposed that Li doping is not necessary to trigger the activity of MgO and undoped MgO itself has been shown good performance in OCM in particularly for stepped surface [20,21]. In fact, there is an explanation that Li doping can be considered as the structural modifier which change the exposed surface of MgO. For example, Luo et al. found that the high index and irregular domain formed on MgO surface after Li doping. Moreover, Schlögl group put forward that the release of methyl radical only become possible under condition of the adsorption of oxygen on surface [22]. This process is highly exothermic which neutralize the highly endothermic of desorption of methyl radical. On the other side, first principles calculations are also extensively performed for OCM study. Eisenberg verified that methane dissociation on stepped MgO surface is exothermic and has a low barrier at DFT-GGA level [23]. Atsushi et al. employed metadynamics based AIMD simulation to compare methane activity on flat MgO(110), stepped MgO(100), and Li doped MgO [24]. In this study, the desorption of CH₃ was not investigated in detail. However, the reaction mechanism is complicated while methane on stepped surface experienced a heterolytic dissociation. In our previous study, DFT calculations also demonstrate that the stepped CaO surface could facilitate the dissociation of methane [25].

Although the importance of stepped surface has been indicated, however the detailed reaction pathway and mechanism are still not well explained. In particularly, what is exactly difference of OCM between flat and stepped surface? In this work, first principles calculations are performed to reveal the reaction process of methane activation on stepped MgO(100). The calculations indicated the importance of interplay between two reactants, CH₄ and O₂. In contrast with previous perception, it is suggested that the co-adsorption of reactants triggered a novel L-H mechanism which show a distinct feature from the previously postulated MvK mechanism. The current work provides a unique insight on the catalytic capability of step site in OCM and new thinking on the further optimization strategy.

2. Computation Setup

The calculations reported here were performed by using periodic, spin-polarized density functional theory (DFT) as implemented in the form of Vienna ab initio simulation package (VASP) [26,27]. For valence electrons, a plane-wave basis set was adopted with an energy cutoff of 400 eV and ionic cores were described with the projector augmented-wave (PAW) method [28,29]. The Revised Perdew-Burke-Ernzerhof (RPBE) [30] functional was used as the exchange-correlation functional approximation which shown better performance in barrier estimation, and used zero damping DFT-D3 method of Grimme for van der Waals correlation correction [31]. Geometry optimization was converged with forces acting on atoms lower than 0.03 eV/Å, whereas the energy threshold defining self-consistency of electron density was set to 10⁻⁶ eV. The reaction pathways with a force tolerance of 0.05 eV/Å and energy barriers were calculated by using the climbing nudged elastic band (CI-NEB) method [32].

The Mono-atomic Stepped MgO(100) surface was modelled by p(7 × 5) five-atomic-layer supercell. All the layers are relaxed. The supercell containing a vacuum space of 10 Å between the slab and its periodic images was used. The Brillouin zone was sampled by a 1 × 1 × 1 Monkhorst-Pack mesh. The reaction barrier was calculated as difference between initial state (IS) and the highest image along pathway.

In order to analyze the methane adsorbed on catalyst, the adsorption energy (ΔE_{ads}) and the reaction energy (ΔE) were defined through following Equation (1):

$$\Delta E_{\text{ads}} = E_{\text{A/catalyst}} - E_{\text{A}} - E_{\text{catalyst}} \quad (1)$$

$$\Delta E = E_{\text{FS}} - E_{\text{IS}}$$

where $E_{A/catalyst}$ is the total energies of the catalyst with the adsorbates (A) including CH_4 and O_2 , $E_{catalyst}$ and E_A are the clean catalyst and the free CH_4 and O_2 , respectively. The E_{FS} and E_{IS} are the total energies of the final state (FS) and the initial state (IS).

3. Results and Discussions

The adsorption of two reactants CH_4 and O_2 molecule has obvious importance to initiate the reaction. The optimized structures of CH_4 and O_2 at mono-atomic stepped $MgO(100)$ surface are shown in Figure 1. The adsorption energies of CH_4 and O_2 were estimated to be -0.25 and -0.25 eV. It can be categorized as weak physisorption as shown in Table S1 in Supporting Information. The C-H bond distance in physisorbed methane molecule did not show noticeable change compared with the counterpart in gas phase. Moreover, one of C-H bonds in methane molecule was pointing to oxygen (Os) at step and distance between H and O_s is 2.50 Å. The adsorption of the oxygen molecule exhibited a different feature. It was revealed that the oxygen molecule basically straddled between the upper step and lower terrace. The bond distance of oxygen molecule was slightly stretched to be 1.26 Å while it is 1.21 Å in gas phase. The oxygens were directed to two magnesium at step and terrace, respectively with a distance of 2.30 and 2.86 Å, respectively. The similar adsorption strength of methane and oxygen molecule yields the possibilities of co-adsorption of methane and oxygen molecule. As indicated in Figure 1, the configurations of methane and oxygen molecule in co-adsorption are very similar to the counterpart in individual adsorption. It is noted that the distance between hydrogen in methane and surface oxygen (O_s) is shortened to be 2.30 Å.

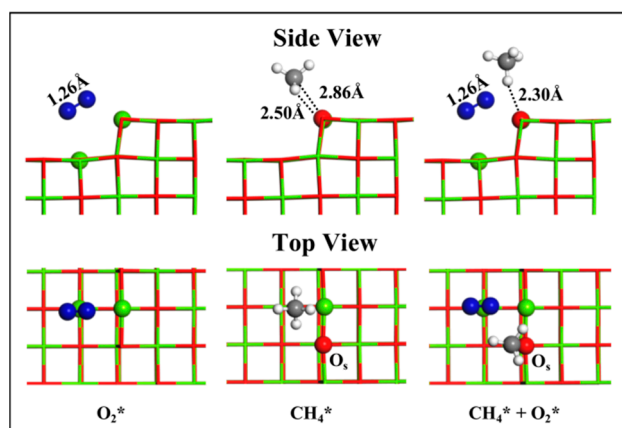


Figure 1. The optimized structures of adsorption and co-adsorption of CH_4 and O_2 . Mg: green; Carbon: gray; Hydrogen: white; Oxygen (oxygen molecule): blue; Oxygen (MgO): red. The same color code applied in following figures, "*" indicated the surface adsorbed species.

It was generally accepted that Mar-Krevelen mechanism is accounted for OCM on MgO catalyst. In this mechanism, methane activation took place firstly and it was followed by re-oxidization by oxygen molecule. The first part of pathway in MvK mechanism was explored as shown in Figure 2 pathway I. From physisorption, one of C-H bond in methane molecule was ruptured at transition state. The abstracted hydrogen almost sits in middle between carbon and oxygen at step with a distance of 1.40 and 1.28 Å, respectively. It is evident that the C-H bond is completely broken. The barrier (TS1) was calculated to be 0.54 eV. After TS1, the dissociated fragments, CH_3 and H, separately bind at Mg-O pair at step with a distance of 2.18 and 0.99 Å, respectively. The release of CH_3 from catalyst was identified to be the most demanding step as desorption is up to 3.18 eV. The significant energy request seemed to justify the needs of the high temperature in OCM reaction. Nevertheless, the large uphill desorption significantly inhibited the generation of CH_3 which influenced the yields of C_2 product.

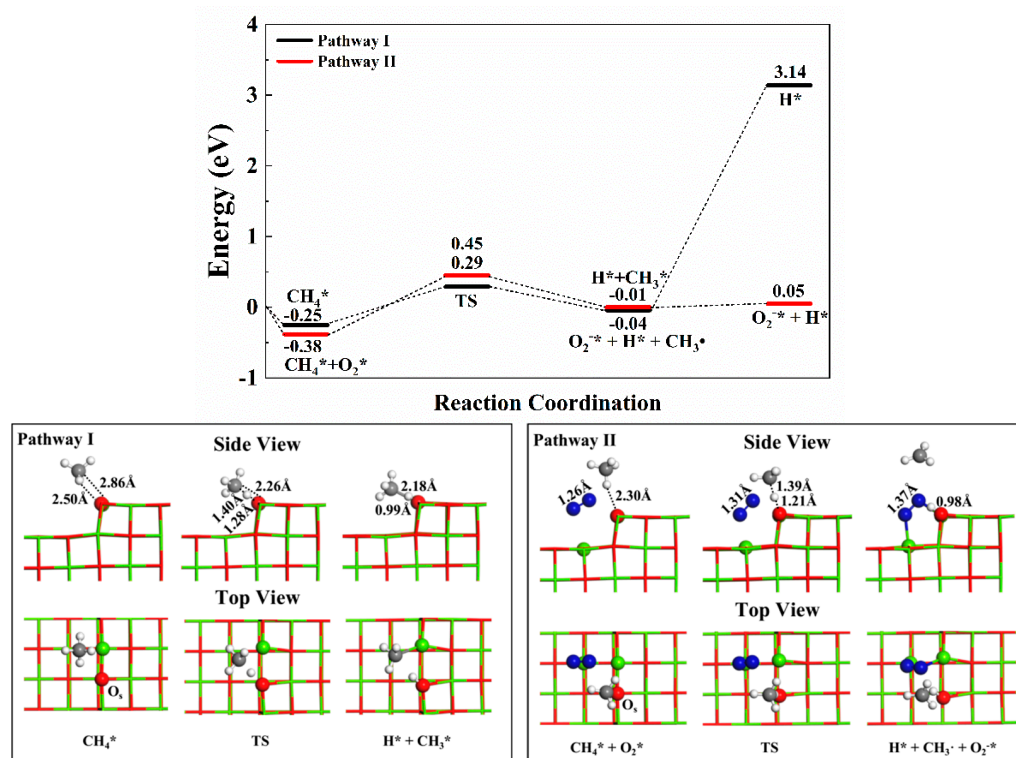


Figure 2. The reaction pathway of CH₃ radical generation and key configurations along reaction pathway. "*" indicated the surface adsorbed species.

The calculations indicated that the release of CH₃ radical was very difficult, based on MvK mechanism. The observations prompted that the possible alternative mechanism to be explored to circumvent this obstacle. The co-adsorption of methane and oxygen molecule brings up another starting configuration. As shown in Figure 2 pathway II, both methane and oxygen molecule simultaneously stay above steps. At transition state (TS1), one hydrogen detached from methane molecule approached oxygen site. The distance between hydrogen and oxygen is calculated to be 1.21 Å. Meanwhile, oxygen molecule is stretched, and one oxygen atom come close to Mg site adjacent to surface oxygen site which abstracted hydrogen. On the other hand, the calculated barrier is slightly increased compared with the one on MvK pathway which is 0.83 eV. After C-H broken, the resulted CH₃ radical was directly release into gas phase. Hence, demanding desorption energy for CH₃ was avoided on this pathway. The re-adsorption of CH₃ is prevented in partly attributed to the Mg site block by the oxygen molecule. Moreover, the oxygen molecule is further elongated to be 1.37 Å. Therefore, the activation of oxygen molecule significantly undermines the reactivity of Mg-O site at step which leads to the facile desorption of CH₃. It is noted that oxygen is not necessary to become adsorbed surface superoxide as proposed in previous study [22].

The striking difference between two pathways shown in Figure 2 indicated that important role of interplay between methane and oxygen molecule. It might be intuitive to attribute the observed difference to the steric effect caused by oxygen molecule occupied nearest Mg site. Indeed, one oxygen atom from O₂ molecule adsorbed at Mg site after methane dissociation with a bond distance of 1.93 Å. It is reasonable to conclude that steric effect is contributed to desorption of CH₃. On the hand, another nearest Mg site of Os was also explored to bind dissociated CH₃. The calculations indicated that CH₃ can not bind that site either. Hence, there are more pronounced effects other than steric hindrance. As shown in Figure 3, density of states analysis indicated that electronic effect induced by co-adsorption along pathway. The obvious difference around Fermi level were found for the transition and final states. Specifically, there are unpaired electrons shown on pathways

II. In contrast, the system was kept as closed-shell along pathway. This rendered the improved stability of configurations along pathway I which consequently cost more energy for CH₃ radical desorption. The facile desorption of CH₃ radical is also evident from charge analysis as shown in Table 1. The charge on CH₃ is significantly reduced on Pathway II compared with the counterpart on Pathway I. The reduced charges weaken the interaction between CH₃ and the positive charged Mg site at step which enhanced desorption. The charges from hydrogen were transferred to oxygen molecule on Pathway II.

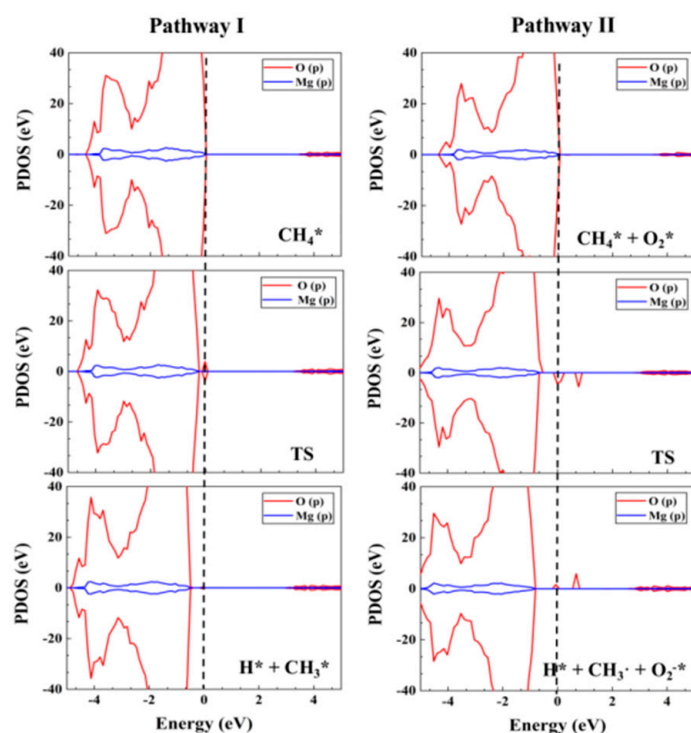


Figure 3. The partial density of states analysis of initial, transition state, and final structures on pathway I and II. “*” indicated the surface adsorbed species.

Table 1. Bader charge analysis of key species during the C-H bond breaking. H and CH₃ represented the dissociated fragments from methane activation.

	$\Delta Q(\text{H})/e$	$\Delta Q(\text{CH}_3)/e$	$\Delta Q(\text{O}_2)/e$
Pathway I	0.69	−0.66	
Pathway II	0.73	0.05	−0.65

4. Conclusions

In this work, a novel mechanism which initiated from co-adsorption of methane and oxygen molecule is verified which outperform conventional MvK mechanism regarding CH₃ radical generation. The enhancements are induced from the effectively interactions between two reactants. The syngenetic effects can be attributed to both steric and electronic effects. The simultaneously oxygen adsorption caused site block and reduced reactivity of Mg-O pair which lead to facile desorption of CH₃ radical. The electronic effects facilitated charge transfer. Moreover, the unique configuration of step sites stabilized the co-adsorption which is not feasible on flat surface. The newly proposed L-H-like mechanism further complement the understandings of reaction process. The current work makes an important contribution to explain of experimental observation in OCM and supply new insight on the mechanism which pave ways to further improve performance.

Supplementary Materials: The following supporting information can be downloaded at: <https://www.mdpi.com/article/10.3390/catal12080903/s1>, Table S1: The optimized bond distance and adsorption energies of CH₄ and O₂ molecular adsorbed on the Stepped MgO(100); Table S2: The optimized bond distance and bader charge along the reaction pathway of the first C-H bond breaking on the Stepped MgO(100); Scheme S1: The schematic illustration OCM reaction mechanism. (a) conventional MvK (b) proposed L-H.

Author Contributions: Conceptualization: X.S. and Z.Z., Investigation: X.S., Y.L. and X.L.; Formal Analysis: Z.Y. and B.L.; Writing: X.S. and Z.Z. All authors have read and agreed to the published version of the manuscript.

Funding: This work is supported by National Natural Science Foundation of China (22172100, 91845201) and Liaoning Natural Science Foundation (2019-ZD-0908). The support from Engineering Technology Research Center of Catalysis for Energy and Environment, Major Platform for Science and Technology of the Universities in Liaoning Province, Liaoning Province Key Laboratory for Highly Efficient Conversion and Clean Utilization of Oil and Gas Resources, and Engineering Research Center for Highly Efficient Conversion and Clean Use of Oil and Gas Resources of Liaoning Province are highly appreciated.

Conflicts of Interest: The authors declare no conflict of interest.

References

- Galadima, A.; Muraza, O. Revisiting the Oxidative Coupling of Methane to Ethylene in the Golden Period of Shale Gas: A Review. *J. Ind. Eng. Chem.* **2016**, *37*, 1–13. [[CrossRef](#)]
- Li, X.; Pei, C.; Gong, J. Shale Gas Revolution: Catalytic Conversion of C₁–C₃ Light Alkanes to Value-Added Chemicals. *Chem* **2021**, *7*, 1755–1801. [[CrossRef](#)]
- Sirola, J.J. The Impact of Shale Gas in the Chemical Industry. *AIChE J.* **2014**, *60*, 810–819. [[CrossRef](#)]
- Schwarz, H. Chemistry with Methane: Concepts Rather than Recipes. *Angew. Chem. Int. Ed.* **2011**, *50*, 10096–10115. [[CrossRef](#)] [[PubMed](#)]
- Schwach, P.; Pan, X.; Bao, X. Direct Conversion of Methane to Value-Added Chemicals over Heterogeneous Catalysts: Challenges and Prospects. *Chem. Rev.* **2017**, *117*, 8497–8520. [[CrossRef](#)] [[PubMed](#)]
- Amenomiya, Y.; Birss, V.I.; Golezdzinowski, M.; Galuszka, J.; Sanger, A.R. Conversion of Methane by Oxidative Coupling. *Catal. Rev.* **1990**, *32*, 163–227. [[CrossRef](#)]
- Lomonosov, V.I.; Sinev, M.Y. Oxidative Coupling of Methane: Mechanism and Kinetics. *Kinet. Catal.* **2016**, *57*, 647–676. [[CrossRef](#)]
- Michorczyk, B.; Sikora, J.; Kordon-Lapczyńska, B.; Gaweł, D.; Czekaj, I. Raw Biogas as Feedstock for the OCM Process. *Catalysts* **2022**, *12*, 54. [[CrossRef](#)]
- Lunsford, J.H. The Catalytic Oxidative Coupling of Methane. *Angew. Chem. Int. Ed.* **1995**, *34*, 970–980. [[CrossRef](#)]
- Sekine, Y.; Tanaka, K.; Matsukata, M.; Kikuchi, E. Oxidative Coupling of Methane on Fe-Doped La₂O₃ Catalyst. *Energy Fuels* **2009**, *23*, 613–616. [[CrossRef](#)]
- Le Van, T.; Louis, C.; Kermarec, M.; Che, M.; Tatibouët, J.M. Temperature and Conversion Dependence of Selectivities in the Oxidative Coupling of Methane on La₂O₃ Catalysts. *Catal. Today* **1992**, *13*, 321–328. [[CrossRef](#)]
- Xiong, J.; Yu, H.; Wei, Y.; Xie, C.; Lai, K.; Zhao, Z.; Liu, J. Metal Ions (Li, Mg, Zn, Ce) Doped into La₂O₃ Nanorod for Boosting Catalytic Oxidative Coupling of Methane. *Catalysts* **2022**, *12*, 713. [[CrossRef](#)]
- Zavvalova, U.; Geske, M.; Horn, R.; Weinberg, G.; Frandsen, W.; Schuster, M.; Schlögl, R. Morphology and Microstructure of Li/MgO Catalysts for the Oxidative Coupling of Methane. *ChemCatChem* **2011**, *3*, 949–959. [[CrossRef](#)]
- Tang, L.; Yamaguchi, D.; Wong, L.; Burke, N.; Chiang, K. The Promoting Effect of Ceria on Li/MgO Catalysts for the Oxidative Coupling of Methane. *Catal. Today* **2011**, *178*, 172–180. [[CrossRef](#)]
- Maitra, A.M.; Campbell, I.; Tyler, R.J. Influence of Basicity on the Catalytic Activity for Oxidative Coupling of Methane. *Appl. Catal. A Gen.* **1992**, *85*, 27–46. [[CrossRef](#)]
- Choudhary, V. Acidity/Basicity of Rare-Earth Oxides and Their Catalytic Activity in Oxidative Coupling of Methane to C₂-Hydrocarbons. *J. Catal.* **1991**, *130*, 411–422. [[CrossRef](#)]
- Kim, J.; Park, L.-H.; Ha, J.-M.; Park, E.D. Oxidative Coupling of Methane over Mn₂O₃-Na₂WO₄/SiC Catalysts. *Catalysts* **2019**, *9*, 363. [[CrossRef](#)]
- Ito, T.; Wang, J.; Lin, C.H.; Lunsford, J.H. Oxidative Dimerization of Methane over a Lithium-Promoted Magnesium Oxide Catalyst. *J. Am. Chem. Soc.* **1985**, *107*, 5062–5068. [[CrossRef](#)]
- Campbell, K.D.; Lunsford, J.H. Contribution of Gas-Phase Radical Coupling in the Catalytic Oxidation of Methane. *J. Phys. Chem.* **1988**, *92*, 5792–5796. [[CrossRef](#)]
- Schwach, P.; Willinger, M.G.; Trunschke, A.; Schlögl, R. Methane Coupling over Magnesium Oxide: How Doping Can Work. *Angew. Chem. Int. Ed.* **2013**, *52*, 11381–11384. [[CrossRef](#)]

21. Schwach, P.; Hamilton, N.; Eichelbaum, M.; Thum, L.; Lunkenbein, T.; Schlögl, R.; Trunschke, A. Structure Sensitivity of the Oxidative Activation of Methane over MgO Model Catalysts: II. Nature of Active Sites and Reaction Mechanism. *J. Catal.* **2015**, *329*, 574–587. [[CrossRef](#)]
22. Kwapien, K.; Paier, J.; Sauer, J.; Geske, M.; Zavyalova, U.; Horn, R.; Schwach, P.; Trunschke, A.; Schlögl, R. Sites for Methane Activation on Lithium-Doped Magnesium Oxide Surfaces. *Angew. Chem. Int. Ed.* **2014**, *53*, 8774–8778. [[CrossRef](#)] [[PubMed](#)]
23. Eisenberg, H.R.; Baer, R. Exothermic Mechanism for the Abstraction of Hydrogen from Methane on Li-Doped MgO. *J. Phys. Chem. C* **2015**, *119*, 196–215. [[CrossRef](#)]
24. Ishikawa, A.; Tateyama, Y. What Is the Active Site for the Oxidative Coupling of Methane Catalyzed by MgO? A Metadynamics-Biased Ab Initio Molecular Dynamics Study. *J. Phys. Chem. C* **2020**, *124*, 6054–6062. [[CrossRef](#)]
25. Sun, X.; Li, B.; Metiu, H. Methane Dissociation on Li-, Na-, K-, and Cu-Doped Flat and Stepped CaO(001). *J. Phys. Chem. C* **2013**, *117*, 7114–7122. [[CrossRef](#)]
26. Kresse, G.; Hafner, J. Ab Initio Molecular Dynamics for Liquid Metals. *Phys. Rev. B* **1993**, *47*, 558–561. [[CrossRef](#)] [[PubMed](#)]
27. Kresse, G.; Furthmüller, J. Efficiency of Ab-Initio Total Energy Calculations for Metals and Semiconductors Using a Plane-Wave Basis Set. *Comput. Mater. Sci.* **1996**, *6*, 15–50. [[CrossRef](#)]
28. Blöchl, P.E. Projector Augmented-Wave Method. *Phys. Rev. B* **1994**, *50*, 17953–17979. [[CrossRef](#)]
29. Kresse, G.; Joubert, D. From Ultrasoft Pseudopotentials to the Projector Augmented-Wave Method. *Phys. Rev. B* **1999**, *59*, 1758–1775. [[CrossRef](#)]
30. Hammer, B.; Hansen, L.B.; Nørskov, J.K. Improved Adsorption Energetics within Density-Functional Theory Using Revised Perdew-Burke-Ernzerhof Functionals. *Phys. Rev. B* **1999**, *59*, 7413–7421. [[CrossRef](#)]
31. Grimme, S.; Ehrlich, S.; Goerigk, L. Effect of the Damping Function in Dispersion Corrected Density Functional Theory. *J. Comput. Chem.* **2011**, *32*, 1456–1465. [[CrossRef](#)] [[PubMed](#)]
32. Henkelman, G.; Uberuaga, B.P.; Jonsson, H. A Climbing Image Nudged Elastic Band Method for Finding Saddle Points and Minimum Energy Paths. *J. Chem. Phys.* **2000**, *113*, 9901–9904. [[CrossRef](#)]